Local variability of vegetation structure increases forest resilience to wildfire

Michael J. Koontz[1,2], Malcolm P. North[2,3], Stephen E. Fick[4,5], Chhaya M. Werner[6], Andrew M. Latimer[2]

[1]Graduate Group in Ecology, University of California, Davis; Davis, CA
[2]Department of Plant Sciences, University of California, Davis; Davis, CA
[3]Pacific Southwest Research Station, U.S.D.A. Forest Service; Mammoth Lakes, CA
[4]U.S. Geological Survey, Southwest Biological Science Center [5]Department of Ecology and Evolutionary Bilogy, University of Colorado, Boulder; Boulder, CO [6]Center for Population Biology, University of California, Davis; Davis, CA

The long-term peristence of forest ecosystems hinges on their resilience to ongoing disturbance. Measurements of resilience for these valuable ecosystems are critical, but are challenging to capture at relevant scales given a forest's temporal longevity and vast spatial extent. Wildfire disturbance plays a key role in structuring the vegetation of many forests, and vegetation structure can feedback to influence wildfire behavior. High fuel loads and hot, dry conditions are known to increase wildfire-induced tree mortality, but local variability of vegetation structure can enable a forest to withstand wildfire disturbance and retain its essential identity and function– a hallmark of a resilient system. We investigate the system-wide generality of variable forest structure confering resilience to the yellow pine/mixed-conifer forest of California's Sierra Nevada mountain range. Vegetation structure and disturbance severity can be reliably detected at system-wide spatiotemporal scales using satellite imagery. We use massively parallel cloud computing and texture analysis of Landsat satellite imagery to generate the most comprehensive dataset of wildfire severity and local variability of vegetation structure in this region to date, spanning its entire spatial extent and a 33-year time series of all known wildfires covering greater than 4 hectares. We find that, on a system-wide scale, greater variability in local forest structure reduces the probability of a high severity wildfire. We find the most support for this relationship at the smallest spatial extent of vegetation structure tested, indicating this phenomenon manifests at a local scale. Variable forest structure thus makes yellow pine/mixed-conifer forest in the Sierra Nevada more resistant to inevitable wildfire disturbance on average, and may increase the probability of long-term forest persistence. Efforts to maintain or increase vegetation structure variability in forests, such as allowing fires to burn under some conditions, should be continued.

Introduction

Biological systems comprising heterogeneous elements can retain their fundamental properties in the face of regular disturbance. This ability of a heterogeneous system to absorb disturbances, reorganize, and to persist within a domain of stability with respect to its identity, structure, function, and feedbacks is termed resilience (Holling 1973; Gunderson 2000; Folke *et al.* 2004; Walker *et al.* 2004). Resilience has been demonstrated in complex biological systems characterized by a variety of different types of "heterogeneity" including genetic diversity (Reusch *et al.* 2005; Agashe 2009; Baskett *et al.* 2009), species diversity (Tilman 1994; Chesson 2000; Cadotte *et al.* 2013), functional diversity (Gazol & Camarero 2016), topoclimatic complexity (Ackerly *et al.* 2010; Lenoir *et al.* 2013), and temporal environmental variation (Questad & Foster 2008). An emerging

paradigm in forest ecology is that spatial heterogeneity in the structure of vegetation on the landscape can confer resilience to disturbances such as wildfire, drought, and insect outbreaks (Stephens *et al.* 2008; North *et al.* 2009; Virah-Sawmy *et al.* 2009). In California, increasing temperature coupled with increasing drought frequency exacerbate water stress on treesduring "hotter droughts" (Park Williams *et al.* 2012; Millar & Stephenson 2015). Further, a century of fire suppression policy has led to drastic densification and homogenization of forest structure in the Sierra Nevada (North *et al.* 2015). Wildfire regimes have changed in these forests such that fires are bigger and burn more at higher severity (Miller & Thode 2007; Cansler & McKenzie 2014; Harvey *et al.* 2016). Changes in wildfire disturbance regimes are particularly suited to catalyze catastrophic shifts in ecosystems because of their feedback with spatial forest heterogeneity at multiple scales. Thus, western North American forests are experiencing novel, "unhealthy" conditions (*sensu* Raffa *et al.* (2009)) that are liable to upset the feedbacks between forest structure and pattern-forming ecological disturbances that historically stabilized the system and made it resilient (Raffa *et al.* 2008; Millar & Stephenson 2015). Forests are of high management priority (Hansen *et al.* 2013; Crowther *et al.* 2015; Millar & Stephenson 2015; Trumbore *et al.* 2015), thus it is critical to understand the mechanisms underlying the effect of spatial heterogeneity in forest structure on forest resilience.

Resilience of forest ecosystems is fundamentally challenging to quantify because forests comprise long-lived species, span large geographic extents, and are affected by disturbances at a very broad range of spatial scales. The ease or difficulty with which a disturbance changes a system's state is resistance, and it is a key component of resilience (Walker *et al.* 2004). In yellow pine/mixed-conifer forests of California's Sierra Nevada mountain range, wildfire disturbance alters the system state at landscape scales with the deaths of overstory trees. Thus, a more resistant forest system should generally experience lower tree mortality when a fire inevitably occurs.

Wildfire severity describes the effect of a wildfire on an ecosystem– often the amount of vegetation mortality (Sugihara & Barbour 2006). Wildfire severity can be measured by comparing pre- and post-fire satellite imagery for a specific area, but this usually requires considerable manual effort for image collation and processing, followed by calibration with field data (Miller & Thode 2007; Miller *et al.* 2009; De Santis *et al.* 2010; Cansler & McKenzie 2012; Veraverbeke & Hook 2013; Parks *et al.* 2014; Prichard & Kennedy 2014; Edwards *et al.* 2018; Fernández-García *et al.* 2018). Efforts to measure severity across broad spatial extents, such as the Monitoring Trends in Burn Severity project (Eidenshink *et al.* 2007), are unsuitably subjective for rigourous scientific analysis though they serve their intended management purpose admirably (Kolden *et al.* 2015). Automated efforts to remotely assess wildfire have arisen, but they tend to focus on more aggregate measures of wildfire such as whether an area burned or the probability that it burned

rather than the severity of the burn (Bastarrika *et al.* (2011); Goodwin & Collett (2014); Boschetti *et al.* (2015); Hawbaker *et al.* (2017) but see Reilly *et al.* (2017) and Parks *et al.* (2018b)). Here, we present a method to automate the measurement of wildfire severity using minimal user inputs: a geometry of interest (a wildfire perimeter or a field plot location) and an alarm date (the date the fire began). This information is readily available in many fire-prone areas (such as California, via the Fire and Resource Assessment Program; http://frap.fire.ca.gov/projects/fire_data/fire_perimeters_index) or could be derived using existing products (such as the Landsat Burned Area Essential Climate Variable product described in Hawbaker *et al.* (2017)).

Vegetation characteristics such as canopy density (Rouse *et al.* 1973; Young *et al.* 2017), moisture content (Asner *et al.* 2015), insect attack (Näsi *et al.* 2015), and even functional diversity (Asner *et al.* 2017) can be measured using remotely-sensed imagery. Texture analysis of imagery can quantify ecologically relevant local environmental heterogeneity across broad spatial extents (Wood *et al.* 2012). Developed for image classification and computer vision, texture analysis characterizes each pixel in an image by a summary statistic of its neighboring pixels (Haralick *et al.* 1973; Conners *et al.* 1984). The value of each pixel represents a measure of local heterogenity within a predefined moving window, and the heterogeneity measurement itself varies across each pixel in the image. Ecologists have successfully used texture measurements to augment predictions of ecosystem properties such as species richness (Huang *et al.* (2014); Stein *et al.* (2014); Tuanmu & Jetz (2015) but see Culbert *et al.* (2012)).

Creation and maintenance of spatial heterogeneity

Forest structure is defined by the size and distribution of trees on the landscape. Differences in tree crown heights characterize vertical structure, while differences in the rooting locations of trees characterizes horizontal structure (North *et al.* 2009). Competition for light, water, and other resources can yield aggregations of trees within favorable microsites, as well as areas containing trees that are more widely spaced trees where resources are more limiting (Clyatt *et al.* 2016). Demographic processes of dispersal, recruitment, and mortality affect forest structure by adding or subtracting whole trees. Reciprocally, forest structure can also influence these pattern-forming processes; for example, vegetation overstory density alters microclimate and changes understory tree demographic rates (Larson & Churchill 2012; De Frenne *et al.* 2013; Ford *et al.* 2013). The stabilizing effects of these reciprocal processes in forests are hallmarks of a resilient system (Folke *et al.* 2004). In the Sierra Nevada range of California, one of the strongest feedbacks between forest structure and pattern-generating ecological process is wildfire, which affects hundreds of thousands to millions of hectares of forested area per year in the Sierra Nevada (Larson & Churchill 2012; Park Williams *et al.* 2012; Millar & Stephenson 2015).

Wildfire interacts dynamically with the forest structure (Westerling *et al.* 2006; Larson & Churchill 2012; Park Williams *et al.* 2012). Wildfire can affect future forest structure by changing demographic rates of individual trees (e.g. increasing growth or germination via increasing light or nitrogen availability), but its most lasting impact to forest structure is in the pattern of killed trees left in its wake (Larson & Churchill 2012). Wildfire behavior is inherently complex and is influenced by local weather, topography, and heterogeneous fuel conditions created by departures from the average fire return interval at any particular place (Sugihara & Barbour 2006; Collins & Stephens 2010). For instance, high tree density and presence of "ladder fuels" in the understory increase the probability of crown fire that kills a high proportion of trees (Agee & Skinner 2005; Stephens *et al.* 2008). A heterogeneous forest can largely avoid overstory tree mortality because a reduced amount of accumulated ladder fuel decreases its ability to get into the crown (where mortality is more likely to result), because wide spacing between tree clumps interrupts high severity fire spread across the landscape, and because small tree clumps with fewer trees don't facilitate self-propagating fire behavior (Graham *et al.* 2004; Scholl & Taylor 2010). In forests with relatively intact fire regimes and heterogeneous stand conditions such as in the Jeffrey pine/mixed-conifer forests of the Sierra San Pedro Mártir in Baja, California, there tends to be reduced vegetation mortality after wildfires compared to fire-suppressed forests (Stephens *et al.* 2008). Thus, forests with heterogeneous structure are predicted to persist due to their resistance to inevitable wildfire disturbance (Graham *et al.* 2004; Moritz *et al.* 2005; Stephens *et al.* 2008). However, it is unclear whether this is true at broad spatial extents, nor is it resolved at what scale variability in forest structure is meaningful for resilience (Kotliar & Wiens 1990).

We use Landsat satellite data and a new image processing approach to calculate wildfire severity for all Sierra Nevada wildfires since 1984 that burned in yellow pine/mixed-conifer forest and covered more than 4 hectares. We calibrate 56 configurations of our algorithmic approach to groud-based wildfire severity measurments, and select the best performing severity metric to generate a comprehensive, system-wide severity dataset. We pair these data with image texture analysis to ask: does spatial variability in forest structure increase the resilience of California yellow pine/mixed-conifer forests by reducing the severity of wildfires? Further, we ask whether the influence of structural heterogeneity on fire severity depends on topographic, fire weather, or other fuel conditions.

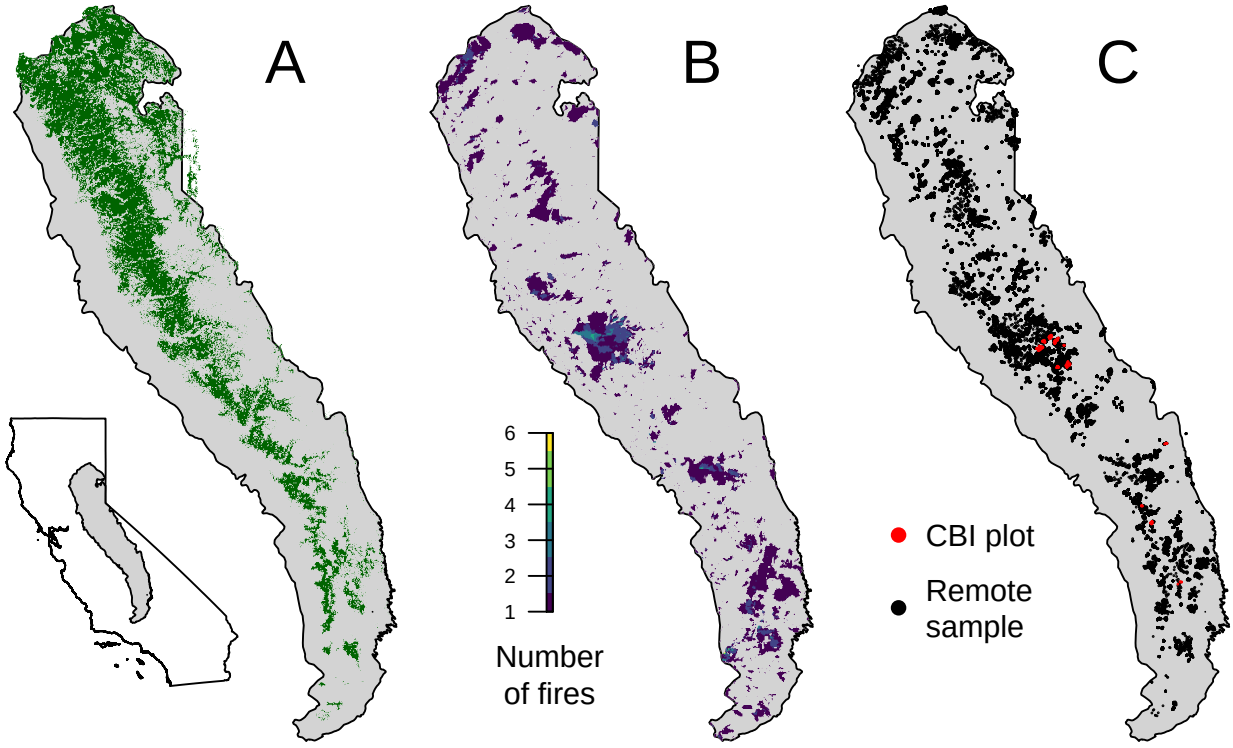

Figure 1: Geographic setting of the study. A) Location of yellow pine/mixed-conifer forests as designated by the Fire Return Interval Departure (FRID) product which, among other things, describes the potential vegetation in an area based on the pre-Euroamerican settlement fire regime. B) Locations of all fires covering greater than 4 hectares that burned in yellow pine/mixed-conifer forest between 1984 and 2017 in the Sierra Nevada mountain range of California according to the State of California Fire Resource and Assessment Program database, the most comprehensive database of fire perimeters of its kind. Colors indicate how many fire perimeters overlapped a given pixel within the study time period. C) (red) Locations of composite burn index (CBI) ground plots used to calibrate the remotely sensed measures of severity. (black) Locations of random samples drawn from 972 unique fires depicted in panel B that were in yellow pine/mixed-conifer forest as depicted in panel A, and which were designated as "burned" by exceeding a threshold relative burn ratio (RBR) determined by calibrating the algorithm presented in this study with ground based CBI measurements.

Methods

Study system

Our study assesses the effect of vegetation structure on wildfire severity in the Sierra Nevada mountain range of California in yellow pine/mixed-conifer forests (Fig. 1). This system is dominated by a mixture of conifer species including ponderosa pine (*Pinus ponderosa*), sugar pine (*Pinus lambertiana*), incense-cedar (*Calocedrus decurrens*), Douglas-fir (*Pseudotsuga menziesii*), white fir (*Abies concolor*), and red fir (*Abies magnifica*) as well as shrubs (Stephens & Collins 2004; Collins *et al.* 2015; Safford & Stevens 2017). We considered "yellow pine/mixed-conifer forest" to be all area designated as a yellow pine, dry mixed conifer, or moist mixed conifer pre-settlement fire regime (PFR) in the USFS Fire Return Interval Departure database (https://www.fs.usda.gov/detail/r5/landmanagement/gis/?cid=STELPRDB5327836). We used the PFR to define our system because it reflects potential vegetation and is less sensitive to recent land cover change (Steel *et al.* 2018). We considered the Sierra Nevada region to be the area within the Sierra Nevada Foothills, the High Sierra Nevada, and the Tehachapi Mountain Area Jepson ecoregions.

The historical range of variation of this system is characterized by relatively low tree density (mean of 143.8 trees ha^{-1}), open canopy (mean of 34.4% canopy cover), and heterogeneous forest struture with highly variable tree density, large and small canopy gaps, and clumps of vegetation dominated by large trees (North 2012; Safford & Stevens 2017). The heterogeneous forest structure manifested at scales ranging from less than one hectare to tens of thousands of hectares, and was maintained by topographic effects on average water availability and frequent, low-severity fire (North 2012; Collins *et al.* 2015; Steel *et al.* 2015). Prior to the era of Euroamerican fire suppression, approximately 5 to 18% of the yellow pine/mixed-conifer system burned annually with an average fire return interval in any given place of about 11 years (North *et al.* 2012; Steel *et al.* 2015; Safford & Stevens 2017). The frequent fire prevented the accumulation of fuel on the ground and reduced the potential for high intensity subsequent fires (Steel *et al.* 2015).

As a result of 150 years of effective fire suppression in this system, overall tree density has increased by a factor of 2.75, canopy cover has increased by 25-49%, and average tree size has decreased by 25 to 40% reflecting a dramatic increase in small trees and loss of large trees (Dolanc *et al.* 2014; McIntyre *et al.* 2014; Stephens *et al.* 2015; Safford & Stevens 2017). This forest infilling has homogenized forest structure on fine scales with the loss of canopy gaps and the fusion of small tree clumps into larger continuous canopy (Lydersen *et al.* 2013). The dense fuel loading and anthropogenic climate change are leading to larger fires and larger patches of complete tree mortality, which homogenizes the forest structure on landscape scales

(Westerling *et al.* 2006; Miller & Safford 2012; Abatzoglou & Williams 2016; Steel *et al.* 2018).

A new approach to remotely sensing wildfire severity

Forest vegetation characteristics and wildfire severity can be reliably detected at long temporal and vast spatial scales from sensors aboard the Landsat series of satellites (Eidenshink *et al.* 2007; Miller & Thode 2007): the Thematic Mapper (TM; Landsat 4 and 5), Enhanced Thematic Mapper Plus (ETM+; Landsat 7), and Operational Land Imager (OLI; Landsat 8). Recent advances in radiometric correction post-processing can compensate for various atmospheric distortions and generate more accurate measurements of surface reflectance in narrow wavelength bands spanning the electromagnetic spectrum (Masek *et al.* 2006; Vermote *et al.* 2016; USGS 2017b, a). Landsat satellites image the entire Earth approximately every 16-days and repeat images of the same area are geometrically coregistered such that overlapping pixels correspond to the same area on the ground. We used Google Earth Engine, a massively parallel cloud-based geographic information system and image hosting platform, for all image collation and processing (Gorelick *et al.* 2017).

To minimize bias in assessing general features of wildfire in this system, it is critical to include small fires in analyses. For instance, Miller and Safford (in prep) found that the modern average fire size was greater than natural range of variation in average fire size in Sierra Nevada yellow pine/mixed-conifer forest when only comparing fires covering greater than a minimum threshold size. However, they found that the modern average fire size was less than the natural range of variation in average fire size when comparing all fires with no size cutoff (Miller and Safford, *in prep*). A key driver of wildfire size is whether initial suppression efforts were successful (Calkin *et al.* 2005). Under fire suppression management, 98% of wildfires are extinguished before they reach 120ha (Calkin *et al.* 2005). The 2% of fires that escape initial suppression often burn in extreme fuel and weather conditions, and these fires constitute 97.5% of the total area burned in this system. Thus, suppression activity exerts a bias on wildfire behavior, whereby the largest fires may not be representative of typical fire behavior though they make up the vast majority of burned area (Safford & Stevens 2017).

We calculated wildfire severity for the most comprehensive digital record of fire perimeters in California: The California Department of Forestry and Fire Protection, Fire and Resource Assessment Program (FRAP) fire perimeter database (http://frap.fire.ca.gov/projects/fire_data/fire_perimeters_index) which includes all known fires that covered more than 4 hectares. Using this database, we quantified severity within each perimeter of 972 wildfires in the Sierra Nevada yellow pine/mixed-conifer forest that burned between 1984 and 2017. Our approach more than doubles the number of fires with severity measurements in this system

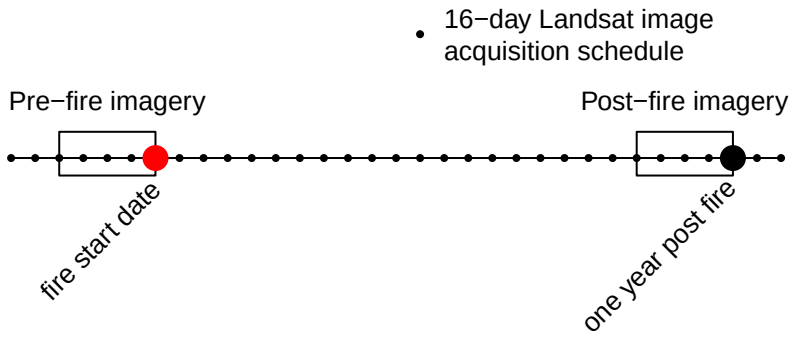

Figure 2: Schematic for how Landsat imagery was assembled in order to make comparisons between pre- and post-fire conditions. This schematic depicts a 64-day window of image collation prior to the fire which comprise the pre-fire image collection. A similar, 64-day window collection of imagery is assembled one year after the pre-fire image collection.

compared to the current standard, which only includes fires covering greater than 80 ha (Miller & Thode 2007; Miller & Safford 2012; Miller *et al.* 2012; Steel *et al.* 2018).

Fetching and processing pre- and postfire imagery

We leveraged the cloud-based data catalog, the large parallel processing system, and the distribution of computation tasks in Google Earth Engine to enable rapid high-throughput analyses using millions of gigabytes of earth observation data (Gorelick *et al.* 2017). Our programmatic assessment of wildfire severity across the 972 Sierra Nevada yellow pine/mixed-conifer fires in the FRAP perimeter database, which required fetching thousands of Landsat images and performing dozens of calculations across them, was automated and took less than an hour to complete.

All Landsat imagery was fetched by "scene"– the atomic unit of image data in the Landsat collection representing an area on the Earth's surface approximately 170 km long by 183 km wide. For each feature, a collection of Landsat scenes was fetched both before and after the fire by defining a date range to search for imagery. The date range for prefire imagery started one day before each feature's alarm date and extended backward in time by a user-defined time window. The date range for postfire imagery was exactly one year after the date range for the prefire search (i.e., one year after the day before the fire, extending backward in time by the same time window). We tested 4 time windows: 16, 32, 48, or 64 days which were chosen to ensure that at least 1, 2, 3, or 4 Landsat images, taken on a 16-day interval, were captured by the date ranges (Fig. 2).

The Landsat archive was filtered to generate a prefire image collection comprising only the Landsat scenes

depicting some part of the feature geometry and within the prefire date range. A postfire image collection was similarly generated by filtering the Landsat archive by the postfire date range and the feature geometry. The Landsat archive we filtered included imagery from Landsat 4, 5, 7, and 8, so each pre- and postfire image collection may contain a mix of scenes from different satellite sources to enhance coverage.

For each image in the pre- and postfire image collections, we masked pixels that were not clear (i.e., clouds, cloud shadows, snow, and water) and calculated standard indices that capture vegetation cover and fire effects such as charring. Normalized difference vegetation index (NDVI; Eq. 1) correlates with vegetation density, canopy cover, and leaf area index (LAI) (Rouse *et al.* 1973). Normalized difference moisture index (NDMI; Eq. 2) correlates with similar vegetation characteristics as NDVI, but doesn't saturate at high levels of foliar biomass (Gao 1996, @Huesca2016). Normalized burn ratio (NBR; Eq. 3) and normalized burn ratio version 2 (NBR2; Eq. 4) respond strongly to fire effects on vegetation (García & Caselles 1991; Key & Benson 2006; Hawbaker *et al.* 2017; USGS 2017a, b).

(1) $ndvi = (nir - red)/(nir + red)$

(2) $ndmi = (nir - swir1)/(nir + swir1)$

(3) $nbr = (nir - swir2)/(nir + swir2)$

(4) $nbr2 = (swir1 - swir2)/(swir1 + swir2)$

Where nir is the near infrared band (band 4 on Landsat 4, 5, and 7; band 5 on Landsat 8) and red is the red band (band 3 on Landsat 4, 5, and 7; band 4 on Landsat 8), $swir1$ is the first short wave infrared band (band 5 on Landsat 4, 5, and 7; band 4 on Landsat 8), $swir2$ is the second short wave infrared band (band 7 on Landsat 4, 5, 7, and 8)

We composited each prefire image collection into a single prefire image using a median reducer, which calculated the median of the unmasked values on a per-pixel basis across the stack of images in the prefire collection. We similarly composited the postfire image collection into a single postfire image. Composite pre- and postfire images can be successfully used to measure wildfire severity instead of using raw, individual scenes (Parks *et al.* 2018b).

Calculating wildfire severity

There is some debate about the most useful measure of remotely-sensed wildfire severity (Miller & Safford 2012; Parks *et al.* 2014; Hawbaker *et al.* 2017), so we calculated the most commonly used metrics to validate against ground-based data. We calculated remotely-sensed wildfire severity using the relative burn ratio

(RBR) (Parks *et al.* 2014), the delta normalized burn ratio (dNBR) (Eidenshink *et al.* 2007; Miller & Thode 2007), the relative delta normalized burn ratio (RdNBR) (Miller & Thode 2007), the delta normalized burn ratio 2 (dNBR2) (Hawbaker *et al.* 2017), the relative delta normalized burn ratio 2 (RdNBR2), and the delta normalized difference vegetation index (dNDVI) (Eidenshink *et al.* 2007). Following the success of the RdNBR metric in other studies, we also calculate an analogous metric using NDVI– the relative delta normalized difference vegetation index (RdNDVI).

We calculated the delta severity indices (dNBR, dNBR2, dNDVI) by subracting the respective postfire indices from the prefire indices (NBR, NBR2, and NDVI) without multiplying by a rescaling constant (e.g., we did not multiply the result by 1000 as in Miller & Thode (2007); Eq. 5). Following Reilly *et al.* (2017), we chose not to correct the delta indices using a phenological offset value (typically calculated as the delta index in homogenous forest patch outside of the fire perimeter), as our approach implicitly accounts for phenology by incorporating multiple cloud-free images across the same time window both before the fire and one year later.

(5) $dI = I_{\text{prefire}} - I_{\text{postfire}}$

We calculated the relative delta severity indices, RdNBR and RdNDVI, by scaling the respective delta indices (dNBR and dNDVI) from Eq. 6 by a square root transformation of the absolute value of the prefire index:

(6) $RdI = \frac{dI}{\sqrt{|I_{\text{prefire}}|}}$

We calculated the relative burn ratio (RBR) following Parks *et al.* (2014) using Eq. 7:

(7) $RBR = \frac{dNBR}{NBR_{\text{prefire}}+1.001}$

Example algorithm outputs are shown in Fig. 3.

Calibrating remotely-sensed wildfire severity with field-measured wildfire severity

We calibrated our remotely-sensed measure of wildfire severity with 208 field measures of overstory tree mortality from two previously published studies (Zhu *et al.* 2006; Sikkink *et al.* 2013) (Fig. 1). The Composite Burn Index (CBI) is a metric of vegetation mortality across several vertical vegetation strata (Key & Benson 2006) and has a long history of use as a standard for calibrating remotely-sensed severity data (Miller & Thode 2007; Miller *et al.* 2009; Cansler & McKenzie 2012; Parks *et al.* 2014, 2018b; Prichard & Kennedy 2014). The CBI ranges from 0 (no fire impacts) to 3 (very high fire impacts) and is an integrated measure of vegetation mortality, scorching, and resprouting assessed in different vertical forest strata within a 30m diameter field plot (Key & Benson 2006). Following Miller & Thode (2007), Miller *et al.* (2009), Parks

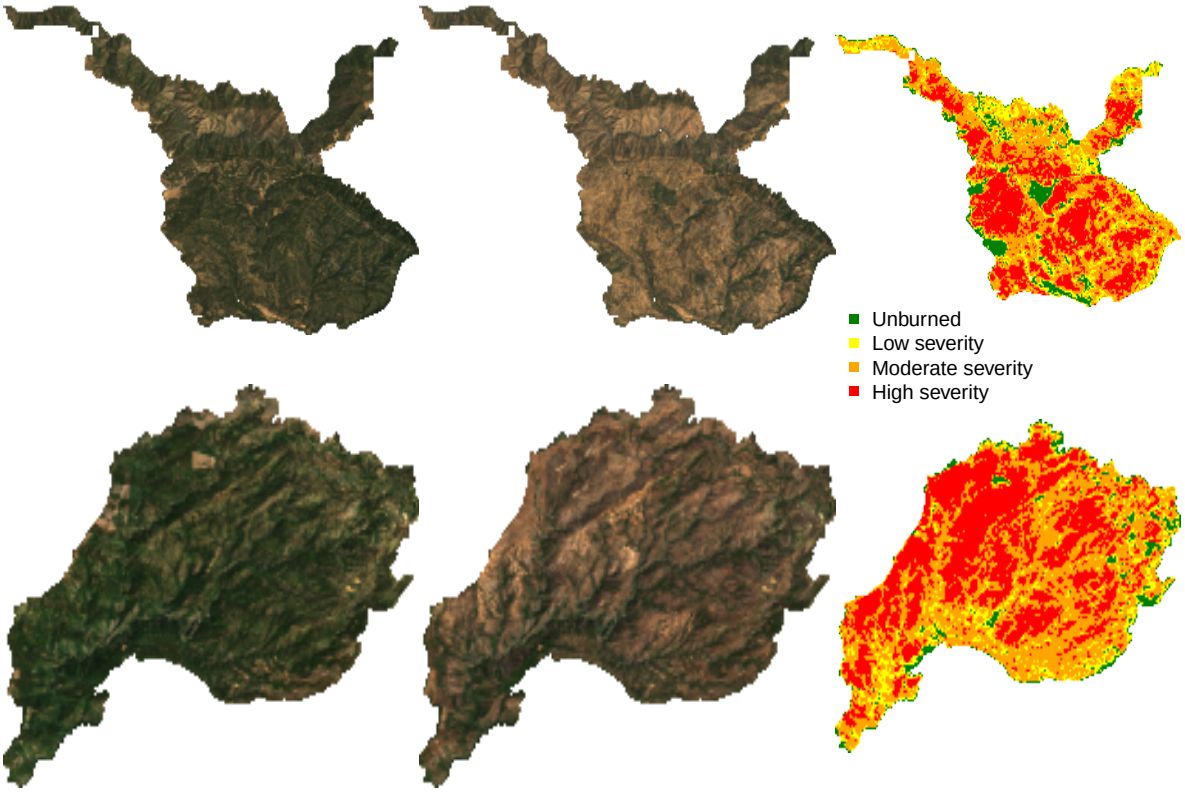

Figure 3: Example algorithm outputs for the Hamm Fire of 1987 (top row) and the American Fire of 2013 (bottom row) showing: prefire true color image (left column), postfire true color image (center column), relative burn ratio (RBR) calculation using a 48-day image collation window before the fire and one year later. For visualization purposes, these algorithm outputs have been resampled to a resolution of 100m x 100m from their original resolution of 30m x 30m. Data used for analyses were sampled from the outputs at the original resolution.

et al. (2014), and Parks *et al.* (2018b), we fit a non-linear model to each remotely-sensed severity metric of the following form:

$$\text{remote\_severity} = \beta_0 + \beta_1 e^{\beta_2 \text{cbi\_overstory}} \quad (8)$$

We fit the model in Eq. 8 for all 7 of our remotely-sensed severity metrics (RBR, dNBR, RdNBR, dNBR2, RdNBR2, dNDVI, RdNDVI) using 4 different time windows from which to collate satellite imagery (16, 32, 48, and 64 days). Following Cansler & McKenzie (2012), Parks *et al.* (2014), and Parks *et al.* (2018b), we used interpolation to extract remotely-sensed severity at the locations of the CBI field plots to better align remote and field measures of severity. We extracted remotely-sensed severity values using both bilinear interpolation, which returns a severity value weighted by the 4 pixel values nearest to the CBI plot location, and bicubic interpolation, which returns a severity value weighted by the 16 pixel values nearest to the CBI plot location. In total, we fit 56 models (7 severity measures, 4 time windows, 2 interpolation methods) and performed five-fold cross validation using the `modelr` and `purrr` packages in R (R Core Team 2018). To compare goodness of model fits with Miller & Thode (2007), Miller *et al.* (2009), and Parks *et al.* (2014), we report the average R^2 value from the five folds for each of the 56 models but note that R^2 for non-linear regressions do not have the same interpretation that they do for linear regression (i.e., R^2 can be greater than 1 for non-linear regression, so it can't be interpreted as the proportion of variation explained by the model).

Remote sensing other conditions

Variability of vegetation

We used texture analysis to calculate a remotely-sensed measure of local forest variability (Haralick *et al.* 1973; Tuanmu & Jetz 2015). Within a moving square neighborhood window with sides of 90m, 150m, 210m, and 270m (corresponding to a moving neighborhood window of 0.81 ha, 2.25 ha, 4.41 ha, and 7.29 ha), we calculated forest variability for each pixel as the standard deviation of the NDVI values of its neighbors (not including itself) (See Fig. 4). NDVI correlates well with foliar biomass, leaf area index, and vegetation density (Rouse *et al.* 1973), so a higher standard deviation of NDVI within a given local neighborhood corresponds to more of a mixture of dense patches and sparsely vegetated patches (see Fig. 4).

Topographic conditions

Elevation data were sourced from the Shuttle Radar Topography Mission (Farr *et al.* 2007), a 1-arc second digital elevation model. Slope and aspect were extracted from the digital elevation model. Per-pixel

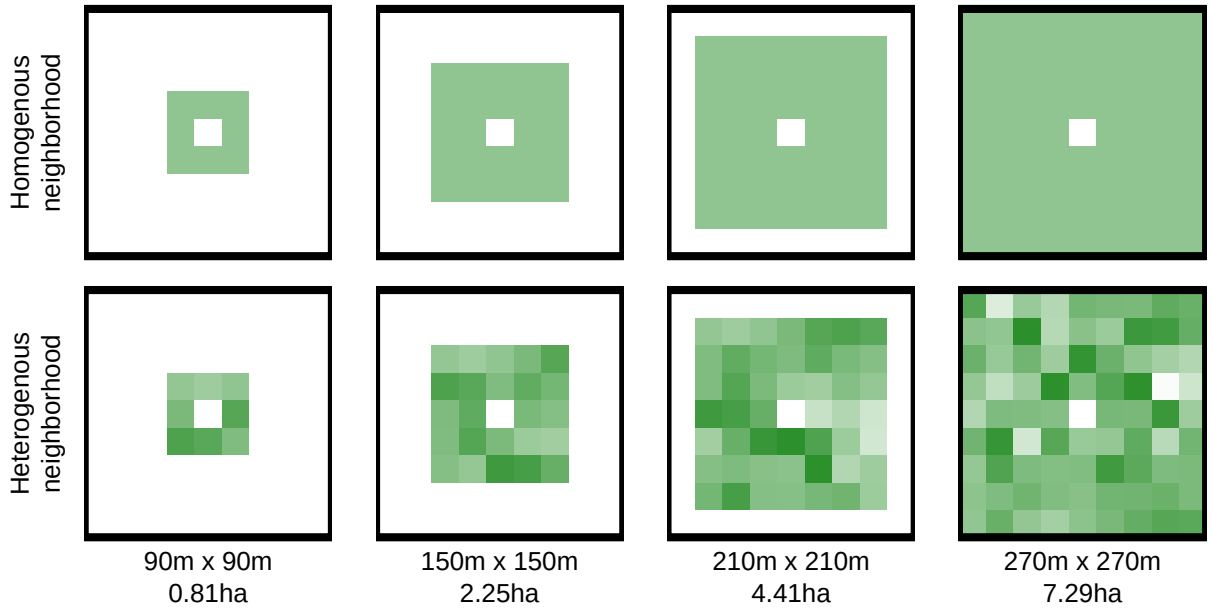

Figure 4: Example of homogenous forest (top row) and heterogenous forest (bottom row) with the same mean NDVI values (~0.6). Each column represents heterogeneity measured using a different neighborhood size.

topographic roughness was calculated as the standard deviation of elevation values within a the same kernel sizes as those used for vegetation heterogeneity (approximately 90m, 150m, 210m, and 270m on a side and not including the central pixel). Some work has shown that terrain ruggedness (Holden *et al.* 2009), and particularly coarser-scale terrain ruggedness (Dillon *et al.* 2011), is an important predictor of wildfire severity.

We used the digital elevation model to calculate the potential annual heat load (Eq. 9 at each pixel, which is an integrated measure of latitude, slope, and a folding transformation of aspect about the northeast-southwest line, such that northeast becomes 0 radians and southwest becomes π radians (McCune & Keon (2002) with correction in McCune (2007)):

$$
\begin{aligned}
aspect_{folded} &= |\pi - |aspect - \frac{5\pi}{4}|| \\
log(pahl) &= \\
&\quad - 1.467 + \\
&\quad 1.582 * cos(latitude)cos(slope) - \\
&\quad 1.5 * cos(aspect_{folded})sin(slope)sin(latitude) - \\
&\quad 0.262 * sin(lat)sin(slope) + \\
&\quad 0.607 * sin(aspect_{folded})sin(slope)
\end{aligned}
\tag{9}
$$

Where *pahl* is the potential annual heat load, $aspect_{folded}$ is a transformation of aspect in radians, and both *latitude* and *slope* are extracted from a digital elevation model with units of radians.

Moisture conditions

The modeled 100-hour fuel moisture data were sourced from the gridMET product, a gridded meteorological product with a daily temporal resolution and a 4km x 4km spatial resolution (Abatzoglou 2013). For our purposes, we calculated 100-hour fuel moisture as the median 100-hour fuel moisture for the 3 days prior to the fire. The 100-hour fuel moisture is a correlate of the regional temperature and moisture which integrates the relative humidity, the length of day, and the amount of precipitation in the previous 24 hours. Thus, this measure is sensitive to multiple hot dry days across the 4km x 4km spatial extent of each grid cell, but not to diurnal variation in relative humidity.

Remote samples

Approximately 100 random points were selected within each FRAP fire perimeter in areas designated as yellow pine/mixed-conifer forest and the values of wildfire severity as well as the values of each covariate were extracted at those points. The random sampling amounted to 54109 total samples across 972 fires.

Modeling the effect of forest variability on severity

We used the Relative Burn Ratio (RBR) calculated using bicubic interpolation within a 48-day window to derive our response variable for analyses of vegetation heterogeneity, as it showed the best correspondence to field severity data measured as average R^2 in the 5-fold cross validation. To quantify resilience, we were most interested in analyzing when the wildfire disturbance resulted in complete or near complete tree morality– when a particular area burned at high severity. Using the non-linear relationship between RBR and CBI from the best performing calibration model, we calculated the threshold RBR that corresponds to "high severity" (CBI value of 2.25). If the severity at a remote sample point was greater than this threshold, the point was scored as a 1. We used the mixed effects logistic regression model described in Eq. 10 to assess the effect of variability in forest structure on the probability of high severity wildfire. We scaled all continuous predictor variables, and treated each individual fire as having a random intercept effect.

$$
\begin{aligned}
severity_{i,j} &\sim Bern(\phi_{i,j}) \\
logit(\phi_{i,j}) = &\ \beta_0 + \\
&\ \beta_{\text{nbhd\_stdev\_NDVI}} * \text{nbhd\_stdev\_NDVI}_i + \\
&\ \beta_{\text{prefire\_NDVI}} * \text{prefire\_NDVI}_i + \\
&\ \beta_{\text{nbhd\_mean\_NDVI}} * \text{nbhd\_mean\_NDVI}_i + \\
&\ \beta_{\text{fm100}} * \text{fm100}_i + \\
&\ \beta_{\text{pahl}} * \text{pahl}_i + \\
&\ \beta_{\text{topographic\_roughness}} * \text{topographic\_roughness}_i + \\
&\ \beta_{\text{nbhd\_stdev\_NDVI*fm100}} * \text{nbhd\_stdev\_NDVI}_i * \text{fm100}_i + \\
&\ \beta_{\text{nbhd\_stdev\_NDVI*prefire\_NDVI}} * \text{nbhd\_stdev\_NDVI}_i * \text{prefire\_NDVI}_i + \\
&\ \beta_{\text{nbhd\_stdev\_NDVI*nbhd\_mean\_NDVI}} * \text{nbhd\_stdev\_NDVI}_i * \text{nbhd\_mean\_NDVI}_i + \\
&\ \beta_{\text{nbhd\_mean\_NDVI*prefire\_NDVI}} * \text{nbhd\_mean\_NDVI}_i * \text{prefire\_NDVI}_i + \\
&\ \gamma_j \\
\gamma_j &\sim \mathcal{N}(0, \sigma_{\text{fire}})
\end{aligned} \tag{10}
$$

Each neighborhood size (90m x 90m, 150m x 150m, 210m x 210m, and 270m x 270m) was substituted in turn for the neighborhood standard deviation of NDVI, neighborhood mean NDVI, and terrain ruggedness covariates to generate a candidate set of 4 models. To assess the scale at which the forest structure variability effect manifests, we compared the 4 candidate models based on different neighborhood sizes using leave-one-out cross validation (LOO cross validation) (Vehtari *et al.* 2016). We inferred that the neighborhood size window used in the best-performing model reflected the scale at which the forest structure variability effect had the most support.

Statistical software and data availability

We used `R` for all statistical analyses (R Core Team 2018). We used the `brms` package to fit mixed effects models in a Bayesian framework which implements the No U-Turn Sampler (NUTS) extension to the Hamiltonian Monte Carlo algorithm (Hoffman & Gelman 2014; Bürkner 2017). We used 4 chains with 3000 samples per chain (1500 warmup samples and 1500 posterior samples) and chain convergence was assessed for each estimated parameter by ensuring Rhat values were less than or equal to 1.01 (Bürkner 2017).

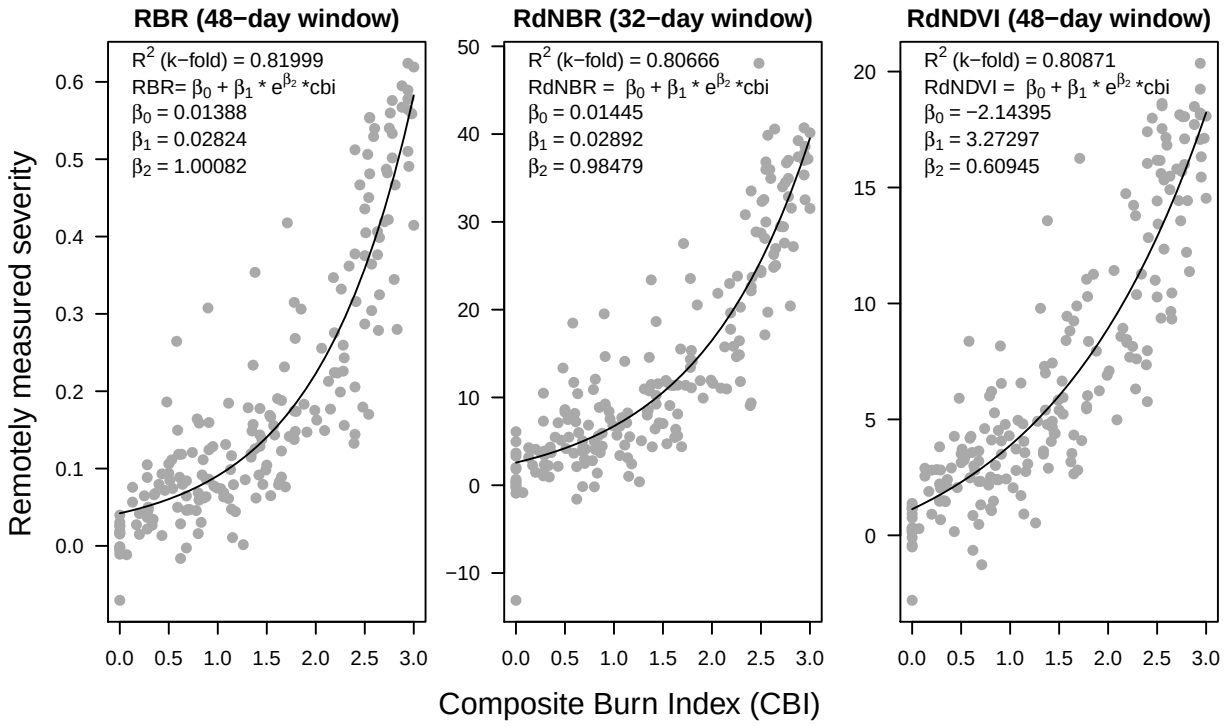

Figure 5: Three top performing remotely-sensed severity metrics based on 5-fold cross validation (relative burn ratio, 48-day window, bicubic interpolation; relative delta normalized burn ratio, 32-day window, bilinear interpolation; and relative delta normalized difference vegetation index, 48-day window, bilinear interpolation) calculated using new automated image collation algorithms, calibrated to 208 field measures of fire severity (composite burn index). See Supplemental Table 1 for performance of all tested models.

Results

A new approach to remotely sensing wildfire severity

We found that the remotely sensed relative burn ratio (RBR) metric of wildfire severity measured across a 48 day interval prior to the wildfire alarm date correlated best with ground based composite burn index (CBI) measurements of severity (5-fold cross validation $R^2 = 0.82$; Fig. 5; Supp. Table 1). Our method to calculate remotely sensed severity using automated Landsat image fetching performs as well or better than most other reported methods that use hand-curation of Landsat imagery (see review in Edwards *et al.* (2018)). Further, several combinations of remotely sensed severity metrics, time windows, and interpolation methods validate well with the ground based severity metrics, including those based on NDVI which is calculated using reflectance in shorter wavelengths than those typically used for measuring severity (Fig. 5). The top three models are depicted in Fig. 5.

Table 1: Model parameter estimates for different neighborhood sizes.

Coefficient	90m x 90m neighborhood	150m x 150m neighborhood	210m x 210m neighborhood	270m x 270m neighborhood
β_0	-2.415 $(-2.588, -2.255)$	-2.432 $(-2.605, -2.271)$	-2.447 $(-2.619, -2.279)$	-2.45 $(-2.618, -2.288)$
$\beta_{\text{nbhd\_stdev\_NDVI}}$	-0.208 $(-0.247, -0.17)$	-0.212 $(-0.255, -0.17)$	-0.203 $(-0.248, -0.158)$	-0.195 $(-0.242, -0.148)$
$\beta_{\text{prefire\_NDVI}}$	1.044 $(0.911, 1.174)$	1.13 $(1.028, 1.229)$	1.141 $(1.057, 1.222)$	1.132 $(1.056, 1.209)$
β_{fm100}	-0.569 $(-0.71, -0.423)$	-0.564 $(-0.709, -0.419)$	-0.561 $(-0.697, -0.428)$	-0.565 $(-0.712, -0.422)$
β_{pahl}	0.239 $(0.208, 0.271)$	0.238 $(0.205, 0.269)$	0.239 $(0.207, 0.269)$	0.24 $(0.209, 0.272)$
$\beta_{\text{topographic\_roughness}}$	-0.01 $(-0.042, 0.022)$	-0.006 $(-0.039, 0.027)$	-0.002 $(-0.037, 0.032)$	-0.002 $(-0.036, 0.033)$
$\beta_{\text{nbhd\_mean\_NDVI}}$	-0.14 $(-0.278, 0.002)$	-0.265 $(-0.381, -0.148)$	-0.293 $(-0.392, -0.193)$	-0.293 $(-0.389, -0.198)$
$\beta_{\text{nbhd\_stdev\_NDVI*prefire\_NDVI}}$	0.125 $(0.029, 0.218)$	0.06 $(-0.013, 0.135)$	0.022 $(-0.045, 0.09)$	0.009 $(-0.054, 0.072)$
$\beta_{\text{nbhd\_stdev\_NDVI*nbhd\_mean\_NDVI}}$	-0.129 $(-0.223, -0.034)$	-0.078 $(-0.151, -0.006)$	-0.03 $(-0.095, 0.035)$	-0.006 $(-0.068, 0.054)$
$\beta_{\text{nbhd\_stdev\_NDVI*fm100}}$	-0.037 $(-0.081, 0.006)$	-0.035 $(-0.078, 0.01)$	-0.03 $(-0.076, 0.014)$	-0.023 $(-0.07, 0.023)$
$\beta_{\text{nbhd\_mean\_NDVI*prefire\_NDVI}}$	-0.573 $(-0.62, -0.526)$	-0.564 $(-0.612, -0.516)$	-0.549 $(-0.596, -0.502)$	-0.537 $(-0.587, -0.49)$

Based on these model comparisons, we used the relative burn ratio (RBR) calculated using a 48-day time window before the fire and bicubic interpolation as our metric of severity. We created the boolean response variable representing whether the sampled point burned at high severity or not by determining whether the RBR exceeded 0.282, the threshold for high severity derived using the non-linear relationship in Eq. 8 (Fig. 5).

Prefire vegetation density, annual heat load, 100-hour fuel moisture, and topographic roughness effects on wildfire severity

We found that the strongest influence on the probability of a forested area burning at high severity is the density of the vegetation, as measured by the prefire NDVI ($\beta_{\text{prefire\_ndvi}} = 1.044$; 95% CI: [0.911, 1.174]) on the log-odds scale; Fig. 6).

For all 4 models using different neighborhood sizes for the heterogeneity and topographic roughness predictors, a greater prefire NDVI led to a greater probability of high severity fire. Potential annual heat load, which integrates aspect, slope, and latitude, also had a strong positive relationship with the probability of a high severity fire ($\beta_{\text{pahl}} = 0.239$; 95% CI: [0.208, 0.271]) Fig. 6).

Areas that were located on southwest facing slopes at lower latitudes tended to be more likely to burn at high severity. We found no effect of local topographic roughness on wildfire severity at any neighborhood size ($\beta_{\text{topographic\_roughness}} = -0.01$; 95% CI: [-0.042, 0.022]) Fig. 6).

100 hour fuel moisture effect on wildfire severity

We found a strong negative relationship between 100 hour fuel moisture and wildfire severity such that increasing fuel moisture was associated with a reduction in the probability of a high severity wildfire ($\beta_{\text{fm100}} = -0.569$; 95% CI: [-0.71, -0.423]) (Fig. 6).

Heterogeneity in vegetation structure effect on wildfire severity

We found strong evidence for an effect of heterogeneity of vegetation structure on the probability of a high severity wildfire.

An increasing heterogeneity of vegetation structure greatly reduced the probability of a high severity wildfire accounting for other variables

Neighborhood size

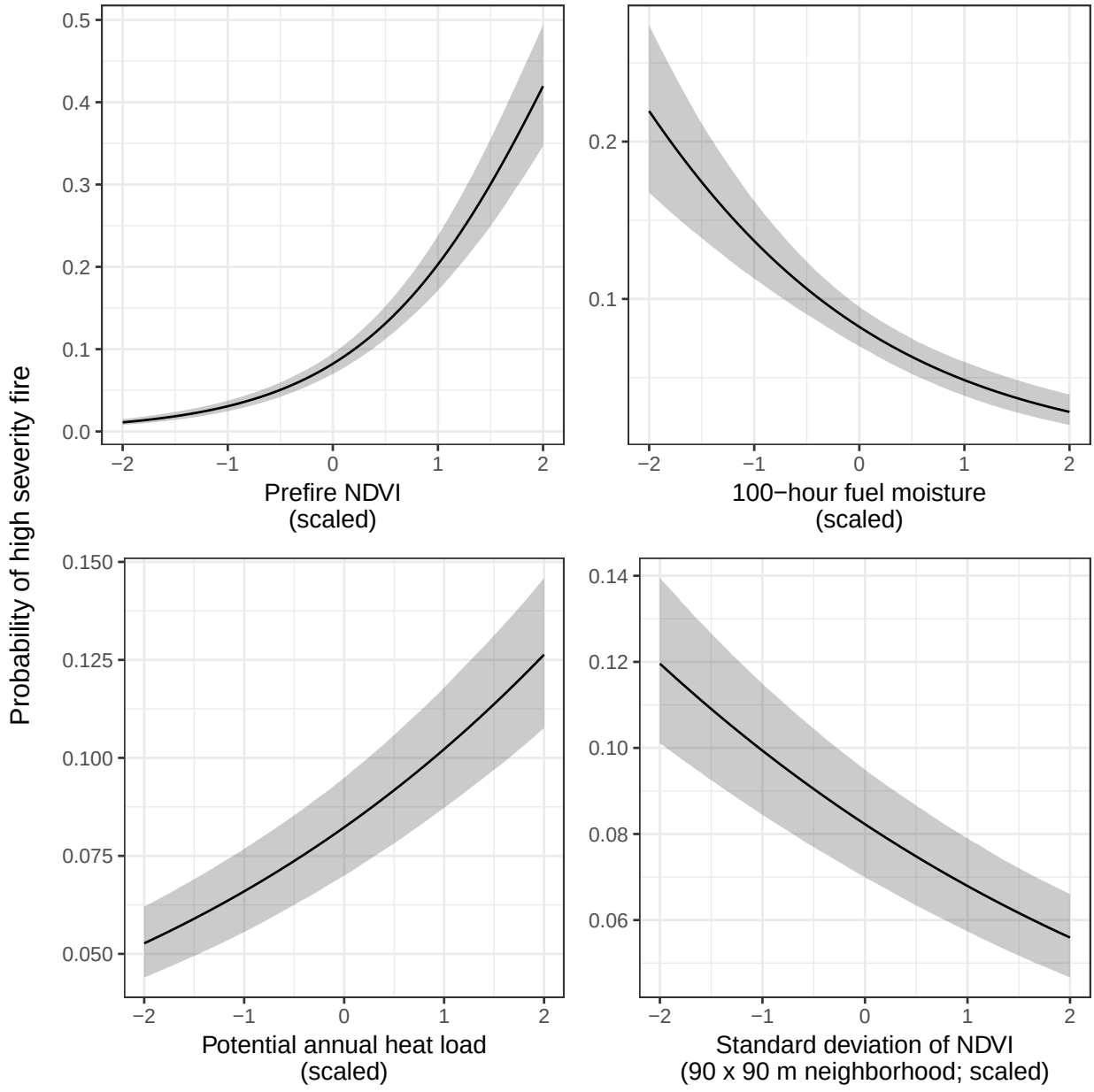

Figure 6: The main effects of the covariates having the strongest relationships with the probability of high severity fire. All depicted relationships derive from the model using the 90m x 90m neighborhood size window for neighborhood standard deviation of NDVI, neighborhood mean of NDVI, and topographic roughness, as this was the best performing model of the four neighborhood sizes tested. The effect sizes of these covariates were similar for each neighborhood size tested.

Table 2: Comparison of four models described in Eq. 10 using different neighborhood sizes for calculating forest heterogeneity (standard deviation of NDVI within the neighborhood), neighborhood mean NDVI, and topographic roughness. LOO is calculated as -2 times the expected log pointwise predictive density (elpd) for a new dataset (Vehtari *et al.* 2016). The Bayesian R^2 is "data-based estimate of the proportion of variance explained for new data" conditional on the model [Gelman2018].

Model	Neighborhood size for heterogeneity measure	LOO (-2*elpd)	ΔLOO to best model	SE of ΔLOO	LOO model weight (%)	Bayesian R^2
1	90m x 90m	40785.77	0.000	NA	100	0.299
2	150m x 150m	40841.80	56.029	14.689	0	0.298
3	210m x 210m	40882.65	96.872	20.943	0	0.297
4	270m x 270m	40911.68	125.906	24.731	0	0.297

Leave-one-out cross validation. Local phenomenon.

Discussion

We developed a new approach to calculating wildfire severity using remotely sensed images from the Landsat series of satellites using a minimal amount of user input– a geometry (i.e., a point location or a perimeter polygon) and a fire start date. We found that the relative burn ratio (RBR) calculated using prefire Landsat images collected over a 48 day period prior to the fire and postfire Landsat images collected over a 48 day period one year after the prefire images validated the best with ground based severity measurements (composite burn index; CBI). We also found that several other remotely sensed measures of severity validated nearly as well with CBI data.

We echo the conclusion of Zhu *et al.* (2006) that the validation of differences between pre- and postfire NDVI to field measured severity data, which uses near infrared reflectance, is comparable to validation using more commonly used severity metrics (e.g., RdNBR and RBR) that rely on short wave infrared reflectance. One immediately operational implication of this is that the increasing availability of low-cost small unhumanned aerial systems (sUAS a.k.a. drones) and near infrared detecting imagers (e.g., those used for agriculture monitoring) may be used to measure wildfire severity at very high spatial resolutions.

Parks *et al.* (2018b) use pre-specified time windows to collate pre- and postfire imagery depending on Arizona, New Mexico, Utah (April through June); all other fires: June through September.

region

Something about time window and bicubic interpolation

We used our new approach to calculate wildfire severity for 972 fires that burned in the Sierra Nevada yellow pine/mixed-conifer forest between 1984 and 2017. We additionally calculated 100 hour fuel moisture, local topographic roughness, potential annual heat load, prefire vegetation density, and the local heterogeneity of prefire vegetation density at 4 neighborhood sizes ranging from 0.81 hectares to 7.29 hectares. We modeled the effect of these variables on wildfire severity and found a strong positive relationship with both prefire vegetation density and potential annual heat load. We found no effect of topographic roughness on wildfire severity. We found a negative effect of 100 hour fuel moisture on severity. We found a strong negative effect of heterogeneity of vegetation structure on wildfire severity, approximately equal to the magnitude of the effect of potential annual heat load.

Effect of high severity

"fire-created chaparral patches are more likely to reburn at high severity, which can result in inhibition of forest succession and a (semi-) permanent conversion to chaparral (Coppoletta et al. 2016, van Wagtendonk et al. 2012). (Safford & Stevens 2017)" Probability of high severity fire and effect on old-growth (Miller & Safford 2017) Live fuel most important factor for Pr(HSF) (Parks *et al.* 2018a)

Mapping finer-scale structure with more resolved instruments (Nomura & Mitchard 2018) Mixed severity fire begets heterogeneous forest structure (Malone *et al.* 2018) Sites lacking prior fire more likely to type convert (Walker *et al.* 2018) High severity begets high severity (Coppoletta *et al.* 2016) Our method may capture some finer scale complexity (Dickinson 2014) Type conversions with large, high severity patches (Stephens *et al.* 2013; Millar & Stephenson 2015)

Caveats

Our method should work best in denser vegetation such as forests, as the signal of a wildfire in other systems can be invisible in a matter of weeks (Goodwin & Collett 2014). This method would also require calibration with field data in other systems, as some severity metrics (such as RBR and RdNBR) have found limited success in other regions (Fernández-García *et al.* 2018).

We have captured a coarse measure of heterogeneity. While we did find that this coarse measure does strongly relate to fire severity, it does not account for fire behavior or spatial pattern forming processes at the individual tree scale. This may still be possible using remotely sensed data at a finer spatial resolution,

but with a cost in temporal resolution and time series depth (e.g., NAIP imagery at 1m resolution but with only 3 total images starting in 2008) (Dickinson *et al.* 2016). Additional metrics of heterogeneity such as vegetation patch size distributions or non-vegetated gap size distributions (Malone *et al.* 2018), may also be more tractable using the finer spatial resolution of NAIP imagery.

FM100 captures local climate conditions, but misses local weather such as strong wind events and plume-dominated fire behavior.

Translating resistance to long term persistance

Texture analysis has been used to measure habitat heterogeneity in ecology, but has only recently gained recognition for its potential to quantify system resilience (Kéfi *et al.* 2014). For instance, increases in the second angular momentum of the configuration of vegetation patches may represent early warning signs of a catastrophic shift in a system whereby it converts to a vegetation-less desert. The change in this particular texture serves as an indicator of system precariousness because it reflects the spatial process by which the system stabilizes. In the case of desertification as a result of increasing grazing pressure, facilitation is the process driving vegetation patch configurations and the increase in spatial variation of those configurations indicates a breakdown in the process itself as the system moves nearer to a bifurcation point between a vegetated and a non-vegetated state. In our case, we measure heterogeneity as a spatial feature that is part of the feedback loop between disturbance and forest spatial structure, so we gain insight into longer-term patterns by measuring a signature of the pattern forming process itself. More work is needed to verify the degree to which the spatial features of mixed-conifer forests– or the spatial features of the disturbances that affect them– capture the

Conclusions

We encourage researchers and managers to make their ground based severity data available with site location (including datum) and the alarm data for the fire the field data is measuring. Cloud-based GIS, central image hosting, and integration with powerful classification tools are sure to advance our ability to measure wildfire severity remotely, automatically, consistently, and at broad spatial scales. While our contribution here demonstrates that satisfactory validation with ground based measurements is possible using simple and well known calculations, we believe that truly groundbreaking abilities to classify wildfire severity would be possible with more open data sharing of ground based severity measures.

While the severity of a wildfire in any given place may be idiosyncratic and controlled by many variables, it is clear that heterogeneous forest structure generally makes mixed-conifer forest in the Sierra Nevada more resistant to this inevitable disturbance under normal fuel moisture conditions. Because a resistant forest is a resilient forest, heterogeneity in forest structure may increase the probability of long-term forest persistence. Given the opposite effect of heterogeneity in extreme fuel moisture conditions and the normalization of what were once considered extreme fuel moisture conditions in a warming world,

1.

Abatzoglou, J.T. (2013). Development of gridded surface meteorological data for ecological applications and modelling. *International Journal of Climatology*, 33, 121–131.

2.

Abatzoglou, J.T. & Williams, A.P. (2016). The impact of anthropogenic climate change on wildfire across western US forests. *Proceedings of the National Academy of Sciences*, In press.

3.

Ackerly, D.D., Loarie, S.R., Cornwell, W.K., Weiss, S.B., Hamilton, H. & Branciforte, R. *et al.* (2010). The geography of climate change: Implications for conservation biogeography. *Diversity and Distributions*, 16, 476–487.

4.

Agashe, D. (2009). The stabilizing effect of intraspecific genetic variation on population dynamics in novel and ancestral habitats. *The American Naturalist*, 174, 255–67.

5.

Agee, J.K. & Skinner, C.N. (2005). Basic principles of forest fuel reduction treatments. *Forest Ecology and Management*, 211, 83–96.

6.

Asner, G.P., Brodrick, P.G., Anderson, C.B., Vaughn, N., Knapp, D.E. & Martin, R.E. (2015). Progressive forest canopy water loss during the 2012–2015 California drought. *Proceedings of the National Academy of Sciences*, 2015, 201523397.

7.

Asner, G.P., Martin, R.E., Knapp, D.E., Tupayachi, R., Anderson, C.B. & Sinca, F. *et al.* (2017). Airborne laser-guided imaging spectroscopy to map forest trait diversity and guide conservation. *Science*, 355, 385–389.

8.

Baskett, M.L., Gaines, S.D. & Nisbet, R.M. (2009). Symbiont diversity may help coral reefs survive moderate climate change. *Ecological Applications*, 19, 3–17.

9.

Bastarrika, A., Chuvieco, E. & Martín, M.P. (2011). Mapping burned areas from landsat TM/ETM+ data with a two-phase algorithm: Balancing omission and commission errors. *Remote Sensing of Environment*, 115, 1003–1012.

10.

Boschetti, L., Roy, D.P., Justice, C.O. & Humber, M.L. (2015). MODIS-Landsat fusion for large area 30m burned area mapping. *Remote Sensing of Environment*, 161, 27–42.

11.

Bürkner, P.-C. (2017). brms : An R Package for Bayesian Multilevel Models Using Stan. *Journal of Statistical Software*, 80.

12.

Cadotte, M., Albert, C.H. & Walker, S.C. (2013). The ecology of differences: Assessing community assembly with trait and evolutionary distances. *Ecology Letters*, 16, 1234–1244.

13.

Calkin, D.E., Gebert, K.M., Jones, J... & Neilson, R.P. (2005). Forest service large fire area burned and suppression expenditure trends, 1970-2002. *Journal of Forestry*, 103, 179–183.

14.

Cansler, C.A. & McKenzie, D. (2012). How robust are burn severity indices when applied in a new region? Evaluation of alternate field-based and remote-sensing methods. *Remote Sensing*, 4, 456–483.

15.

Cansler, C.A. & McKenzie, D. (2014). Climate, fire size, and biophysical setting control fire severity and spatial pattern in the northern Cascade Range, USA. *Ecological Applications*, 24, 1037–1056.

16.

Chesson, P. (2000). Mechanisms of maintenance of species diversity. *Annual Review of Ecology and Systematics*, 31, 343–366.

17.

Clyatt, K.A., Crotteau, J.S., Schaedel, M.S., Wiggins, H.L., Kelley, H. & Churchill, D.J. *et al.* (2016). Historical spatial patterns and contemporary tree mortality in dry mixed-conifer forests. *Forest Ecology and*

Management, 361, 23–37.

18.

Collins, B.M., Lydersen, J.M., Everett, R.G., Fry, D.L. & Stephens, S.L. (2015). Novel characterization of landscape-level variability in historical vegetation structure. *Ecological Applications*, 25, 1167–1174.

19.

Collins, B.M. & Stephens, S.L. (2010). Stand-replacing patches within a 'mixed severity' fire regime: Quantitative characterization using recent fires in a long-established natural fire area. *Landscape Ecology*, 25, 927–939.

20.

Conners, R.W., Trivedi, M.M. & Harlow, C.A. (1984). Segmentation of a high-resolution urban scene using texture operators. *Computer Vision, Graphics, and Image Processing*, 25, 273–310.

21.

Coppoletta, M., Merriam, K.E. & Collins, B.M. (2016). Post-fire vegetation and fuel development influences fire severity patterns in reburns. *Ecological Applications*, 26, 686–699.

22.

Crowther, T.W., Glick, H.B., Covey, K.R., Bettigole, C., Maynard, D.S. & Thomas, S.M. *et al.* (2015). Mapping tree density at a global scale. *Nature*, 525, 201–205.

23.

Culbert, P.D., Radeloff, V.C., St-Louis, V., Flather, C.H., Rittenhouse, C.D. & Albright, T.P. *et al.* (2012). Modeling broad-scale patterns of avian species richness across the Midwestern United States with measures of satellite image texture. *Remote Sensing of Environment*, 118, 140–150.

24.

De Frenne, P., Rodríguez-Sánchez, F., Coomes, D.A., Baeten, L., Verstraeten, G. & Vellend, M. *et al.* (2013). Microclimate moderates plant responses to macroclimate warming. *Proceedings of the National Academy of Sciences of the United States of America*, 110, 18561–5.

25.

De Santis, A., Asner, G.P., Vaughan, P.J. & Knapp, D.E. (2010). Mapping burn severity and burning efficiency in California using simulation models and Landsat imagery. *Remote Sensing of Environment*, 114, 1535–1545.

26.

545 Dickinson, Y. (2014). Landscape restoration of a forest with a historically mixed-severity fire regime: What
546 was the historical landscape pattern of forest and openings? *Forest Ecology and Management*, 331, 264–271.

547 27.

548 Dickinson, Y., Pelz, K., Giles, E. & Howie, J. (2016). Have we been successful? Monitoring horizontal forest
549 complexity for forest restoration projects. *Restoration Ecology*, 24, 8–17.

550 28.

551 Dillon, G.K., Holden, Z.A., Morgan, P., Crimmins, M.A., Heyerdahl, E.K. & Luce, C.H. (2011). Both
552 topography and climate affected forest and woodland burn severity in two regions of the western US, 1984 to
553 2006. *Ecosphere*, 2, art130.

554 29.

555 Dolanc, C.R., Safford, H.D., Dobrowski, S.Z. & Thorne, J.H. (2014). Twentieth century shifts in abundance
556 and composition of vegetation types of the Sierra Nevada, CA, US. *Applied Vegetation Science*, 17, 442–455.

557 30.

558 Edwards, A.C., Russell-Smith, J. & Maier, S.W. (2018). A comparison and validation of satellite-derived fire
559 severity mapping techniques in fire prone north Australian savannas: Extreme fires and tree stem mortality.
560 *Remote Sensing of Environment*, 206, 287–299.

561 31.

562 Eidenshink, J., Schwind, B., Brewer, K., Zhu, Z.-l., Quayle, B. & Howard, S. (2007). A project for monitoring
563 trends in burn severity. *Fire Ecology*, 3, 3–21.

564 32.

565 Farr, T., Rosen, P., Caro, E., Crippen, R., Duren, R. & Hensley, S. *et al.* (2007). The shuttle radar topography
566 mission. *Reviews of Geophysics*, 45, 1–33.

567 33.

568 Fernández-García, V., Santamarta, M., Fernández-Manso, A., Quintano, C., Marcos, E. & Calvo, L. (2018).
569 Burn severity metrics in fire-prone pine ecosystems along a climatic gradient using Landsat imagery. *Remote*
570 *Sensing of Environment*, 206, 205–217.

571 34.

572 Folke, C., Carpenter, S., Walker, B., Scheffer, M., Elmqvist, T. & Gunderson, L. *et al.* (2004). Regime shifts,
573 resilience, and biodiversity in ecosystem management. *Annual Review of Ecology, Evolution, and Systematics*,
574 35, 557–581.

35.

Ford, K.R., Ettinger, A.K., Lundquist, J.D., Raleigh, M.S. & Hille Ris Lambers, J. (2013). Spatial heterogeneity in ecologically important climate variables at coarse and fine scales in a high-snow mountain landscape. *PLoS ONE*, 8, e65008.

36.

Gao, B.C. (1996). NDWI - A normalized difference water index for remote sensing of vegetation liquid water from space. *Remote Sensing of Environment*, 58, 257–266.

37.

García, M.J.L. & Caselles, V. (1991). Mapping burns and natural reforestation using thematic mapper data. *Geocarto International*, 6, 31–37.

38.

Gazol, A. & Camarero, J.J. (2016). Functional diversity enhances silver fir growth resilience to an extreme drought. *Journal of Ecology*.

39.

Goodwin, N.R. & Collett, L.J. (2014). Development of an automated method for mapping fire history captured in Landsat TM and ETM+ time series across Queensland, Australia. *Remote Sensing of Environment*, 148, 206–221.

40.

Gorelick, N., Hancher, M., Dixon, M., Ilyushchenko, S., Thau, D. & Moore, R. (2017). Remote Sensing of Environment Google Earth Engine : Planetary-scale geospatial analysis for everyone. *Remote Sensing of Environment*, 202, 18–27.

41.

Graham, R.T., McCaffrey, S. & Jain, T.B. (2004). *Science basis for changing forest structure to modify wildfire behavior and severity* (No. April). US Department of Agriculture, Forest Service, Rokcy Mountain Research Station, Fort Collins, CO.

42.

Gunderson, L.H. (2000). Ecological resilience– in theory and application. *Annual Review of Ecology and Systematics*, 31, 425–439.

43.

Hansen, M.C., Potapov, P.V., Moore, R., Hancher, M., Turubanova, S.A. & Tyukavina, A. (2013). High-

605 resolution global maps of 21st-century forest cover change. *Science*, 342, 850–853.

606 44.

607 Haralick, R.M., Shanmugam, K. & Dinstein, I. (1973). Textural Features for Image Classification. *IEEE*
608 *Transactions on Systems, Man, and Cybernetics*, SMC-3, 610–621.

609 45.

610 Harvey, B.J., Donato, D.C. & Turner, M.G. (2016). Drivers and trends in landscape patterns of stand-replacing
611 fire in forests of the US Northern Rocky Mountains (1984–2010). *Landscape Ecology*, 31, 2367–2383.

612 46.

613 Hawbaker, T.J., Vanderhoof, M.K., Beal, Y.J., Takacs, J.D., Schmidt, G.L. & Falgout, J.T. *et al.* (2017).
614 Mapping burned areas using dense time-series of Landsat data. *Remote Sensing of Environment*, 198, 504–522.

615 47.

616 Hoffman, M.D. & Gelman, A. (2014). The No-U-Turn Sampler: Adaptively Setting Path Lengths in
617 Hamiltonian Monte Carlo. *Journal of Machine Learning Research*, 15, 1593–1623.

618 48.

619 Holden, Z.A., Morgan, P. & Evans, J.S. (2009). A predictive model of burn severity based on 20-year satellite-
620 inferred burn severity data in a large southwestern US wilderness area. *Forest Ecology and Management*, 258,
621 2399–2406.

622 49.

623 Holling, C.S. (1973). Resilience and Stability of Ecological Systems. *Annual Review of Ecology and Systematics*,
624 4, 1–23.

625 50.

626 Huang, Q., Swatantran, A., Dubayah, R. & Goetz, S.J. (2014). The influence of vegetation height heterogeneity
627 on forest and woodland bird species richness across the United States. *PLoS ONE*, 9.

628 51.

629 Huesca, M., García, M., Roth, K.L., Casas, A. & Ustin, S.L. (2016). Canopy structural attributes derived
630 from AVIRIS imaging spectroscopy data in a mixed broadleaf/conifer forest. *Remote Sensing of Environment*,
631 182, 208–226.

632 52.

633 Key, C.H. & Benson, N.C. (2006). Landscape assessment: Sampling and analysis methods. *USDA Forest*
634 *Service General Technical Report RMRS-GTR-164-CD*, 1–55.

635 53.

636 Kéfi, S., Guttal, V., Brock, W.A., Carpenter, S.R., Ellison, A.M. & Livina, V.N. *et al.* (2014). Early warning
637 signals of ecological transitions: Methods for spatial patterns. *PLoS ONE*, 9, 10–13.

638 54.

639 Kolden, C.A., Smith, A.M.S. & Abatzoglou, J.T. (2015). Limitations and utilisation of Monitoring Trends in
640 Burn Severity products for assessing wildfire severity in the USA. *International Journal of Wildland Fire*, 24,
641 1023–1028.

642 55.

643 Kotliar, N.B. & Wiens, J. a. (1990). Multiple Scales of Patchiness and Patch Structure: A Hierarchical
644 Framework for the Study of Heterogeneity. *Oikos*, 59, 253–260.

645 56.

646 Larson, A.J. & Churchill, D. (2012). Tree spatial patterns in fire-frequent forests of western North America,
647 including mechanisms of pattern formation and implications for designing fuel reduction and restoration
648 treatments. *Forest Ecology and Management*, 267, 74–92.

649 57.

650 Lenoir, J., Graae, B.J., Aarrestad, P.A., Alsos, I.G., Armbruster, W.S. & Austrheim, G. *et al.* (2013). Local
651 temperatures inferred from plant communities suggest strong spatial buffering of climate warming across
652 Northern Europe. *Global Change Biology*, 19, 1470–1481.

653 58.

654 Lydersen, J.M., North, M.P., Knapp, E.E. & Collins, B.M. (2013). Quantifying spatial patterns of tree groups
655 and gaps in mixed-conifer forests: Reference conditions and long-term changes following fire suppression and
656 logging. *Forest Ecology and Management*, 304, 370–382.

657 59.

658 Malone, S.L., Fornwalt, P.J., Battaglia, M.A., Chambers, M.E., Iniguez, J.M. & Sieg, C.H. (2018). Mixed-
659 severity fire fosters heterogeneous spatial patterns of conifer regeneration in a dry conifer forest. *Forests*,
660 9.

661 60.

662 Masek, J.G., Vermote, E.F., Saleous, N.E., Wolfe, R., Hall, F.G. & Huemmrich, K.F. *et al.* (2006). A Landsat
663 Surface Reflectance Dataset. *IEEE Geoscience and Remote Sensing Letters*, 3, 68–72.

664 61.

McCune, B. (2007). Improved estimates of incident radiation and heat load using non-parametric regression against topographic variables. *Journal of Vegetation Science*, 18, 751–754.

62.

McCune, B. & Keon, D. (2002). Equations for potential annual direct incident radiation and heat load. *Journal of Vegetation Science*, 13, 603–606.

63.

McIntyre, P.J., Thorne, J.H., Dolanc, C.R., Flint, A.L., Flint, L.E. & Kelly, M. *et al.* (2014). Twentieth-century shifts in forest structure in California: Denser forests, smaller trees, and increased dominance of oaks. *Proceedings of the National Academy of Sciences*, 112, 1458–1463.

64.

Millar, C.I. & Stephenson, N.L. (2015). Temperate forest health in an era of emerging megadisturbance. *Science*, 349, 823–826.

65.

Miller, J.D., Knapp, E.E., Key, C.H., Skinner, C.N., Isbell, C.J. & Creasy, R.M. *et al.* (2009). Calibration and validation of the relative differenced Normalized Burn Ratio (RdNBR) to three measures of fire severity in the Sierra Nevada and Klamath Mountains, California, USA. *Remote Sensing of Environment*, 113, 645–656.

66.

Miller, J.D. & Safford, H. (2012). Trends in wildfire severity: 1984 to 2010 in the Sierra Nevada, Modoc Plateau, and southern Cascades, California, USA. *Fire Ecology*, 8, 41–57.

67.

Miller, J.D. & Safford, H.D. (2017). Corroborating evidence of a pre-euro-American low-to moderate-severity fire regime in yellow pine–mixed conifer forests of the sierra Nevada, California, USA. *Fire Ecology*, 13, 58–90.

68.

Miller, J.D., Skinner, C.N., Safford, H.D., Knapp, E.E. & Ramirez, C.M. (2012). Trends and causes of severity, size, and number of fires in northwestern California, USA. *Ecological Applications*, 22, 184–203.

69.

Miller, J.D. & Thode, A.E. (2007). Quantifying burn severity in a heterogeneous landscape with a relative version of the delta Normalized Burn Ratio (dNBR). *Remote Sensing of Environment*, 109, 66–80.

70.

Moritz, M.A., Morais, M.E., Summerell, L.A., Carlson, J.M. & Doyle, J. (2005). Wildfires, complexity, and

highly optimized tolerance. *Proceedings of the National Academy of Sciences*, 102, 17912–7.

71.

Näsi, R., Honkavaara, E., Lyytikäinen-Saarenmaa, P., Blomqvist, M., Litkey, P. & Hakala, T. *et al.* (2015). Using UAV-based photogrammetry and hyperspectral imaging for mapping bark beetle damage at tree-level. *Remote Sensing*, 7, 15467–15493.

72.

Nomura, K. & Mitchard, E. (2018). More Than Meets the Eye: Using Sentinel-2 to Map Small Plantations in Complex Forest Landscapes. *Remote Sensing*, 10, 1693.

73.

North, M. (2012). *Managing Sierra Nevada Forests* (No. March). U. S. Department of Agriculture, Forest Service, Pacific Southwest Research Station; USDA Forest Service, Albany, CA.

74.

North, M., Collins, B.M. & Stephens, S. (2012). Using Fire to Increase the Scale, Benefits, and Future Maintenance of Fuels Treatments. *Journal of Forestry*, 110, 392–401.

75.

North, M.P., Stephens, S.L., Collins, B.M., Agee, J.K., Aplet, G. & Franklin, J.F. *et al.* (2015). Reform forest fire managment. *Science*, 349, 1280–1281.

76.

North, M., Stine, P., Hara, K.O., Zielinski, W. & Stephens, S. (2009). An Ecosystem Management Strategy for Sierran Mixed- Conifer Forests. *General Technical Report PSW-GTR-220*, 1–49.

77.

Park Williams, A., Allen, C.D., Macalady, A.K., Griffin, D., Woodhouse, C.A. & Meko, D.M. *et al.* (2012). Temperature as a potent driver of regional forest drought stress and tree mortality. *Nature Climate Change*, 3, 292–297.

78.

Parks, S.A., Dillon, G.K. & Miller, C. (2014). A new metric for quantifying burn severity: The relativized burn ratio. *Remote Sensing*, 6, 1827–1844.

79.

Parks, S.A., Holsinger, L.M., Panunto, M.H., Jolly, W.M., Dobrowski, S.Z. & Dillon, G.K. (2018a). High-severity fire: Evaluating its key drivers and mapping its probability across western US forests. *Environmental*

Research Letters, 13.

80.

Parks, S., Holsinger, L., Voss, M., Loehman, R. & Robinson, N. (2018b). Mean Composite Fire Severity Metrics Computed with Google Earth Engine Offer Improved Accuracy and Expanded Mapping Potential. *Remote Sensing*, 10, 879.

81.

Prichard, S.J. & Kennedy, M.C. (2014). Fuel treatments and landform modify landscape patterns of burn severity in an extreme fire event. *Ecological Applications*, 24, 571–590.

82.

Questad, E.J. & Foster, B.L. (2008). Coexistence through spatio-temporal heterogeneity and species sorting in grassland plant communities. *Ecology Letters*, 11, 717–726.

83.

R Core Team. (2018). *R: A language and environment for statistical computing. http://www.r-project.org/*. R Foundation for Statistical Computing, Vienna, Austria.

84.

Raffa, K.F., Aukema, B., Bentz, B.J., Carroll, A., Erbilgin, N. & Herms, D.A. *et al.* (2009). A literal use of 'forest health' safeguards against misuse and misapplication. *Journal of Forestry*, 276–277.

85.

Raffa, K.F., Aukema, B.H., Bentz, B.J., Carroll, A.L., Hicke, J.A. & Turner, M.G. *et al.* (2008). Cross-scale drivers of natural disturbances prone to anthropogenic amplification: The dynamics of bark beetle eruptions. *BioScience*, 58, 501.

86.

Reilly, M.J., Dunn, C.J., Meigs, G.W., Spies, T.A., Kennedy, R.E. & Bailey, J.D. *et al.* (2017). Contemporary patterns of fire extent and severity in forests of the Pacific Northwest, USA (1985-2010). *Ecosphere*, 8.

87.

Reusch, T.B.H., Ehlers, A., Hämmerli, A. & Worm, B. (2005). Ecosystem recovery after climatic extremes enhanced by genotypic diversity. *Proceedings of the National Academy of Sciences*, 102, 2826–2831.

88.

Rouse, J.W., Hass, R.H., Schell, J. & Deering, D. (1973). Monitoring vegetation systems in the great plains with ERTS. *Third Earth Resources Technology Satellite (ERTS) symposium*, 1, 309–317.

89.

Safford, H.D. & Stevens, J.T. (2017). Natural Range of Variation (NRV) for yellow pine and mixed conifer forests in the bioregional assessment area, including the Sierra Nevada, southern Cascades, and Modoc and Inyo National Forests. *Gen. Tech. Rep. PSW-GTR-2562*, 1–151.

90.

Scholl, A.E. & Taylor, A.H. (2010). Fire regimes, forest change, and self-organization in an old-growth mixed-conifer forest, Yosemite National Park, USA. *Ecological Applications*, 20, 362–380.

91.

Sikkink, P.G., Dillon, G.K., Keane, R.E., Morgan, P., Karau, E.C. & Holden, Z.A. *et al.* (2013). *Composite Burn Index (CBI) data and field photos collected for the FIRESEV project, western United States.* Forest Service Research Data Archive, Fort Collins, CO.

92.

Steel, Z.L., Koontz, M.J. & Safford, H.D. (2018). The changing landscape of wildfire: Burn pattern trends and implications for California's yellow pine and mixed conifer forests. *Landscape Ecology*, 33, 1159–1176.

93.

Steel, Z.L., Safford, H.D. & Viers, J.H. (2015). The fire frequency-severity relationship and the legacy of fire suppression in California forests. *Ecosphere*, 6, 1–23.

94.

Stein, A., Gerstner, K. & Kreft, H. (2014). Environmental heterogeneity as a universal driver of species richness across taxa, biomes and spatial scales. *Ecology Letters*, 17, 866–880.

95.

Stephens, S.L., Agee, J.K., Fulé, P.Z., North, M.P., Romme, W.H. & Swetnam, T.W. *et al.* (2013). Managing forests and fire in changing climates. *Science*, 342, 41–2.

96.

Stephens, S.L. & Collins, B.M. (2004). Fire regimes of mixed conifer forests in the North-Central Sierra Nevada at multiple scales. *Northwest Science*, 78, 12–23.

97.

Stephens, S.L., Fry, D.L. & Franco-Vizcaíno, E. (2008). Wildfire and spatial patterns in forests in northwestern Mexico: The United States wishes it had similar fire problems. *Ecology and Society.*

98.

785 Stephens, S.L., Lydersen, J.M., Collins, B.M., Fry, D.L. & Meyer, M.D. (2015). Historical and current
786 landscape-scale ponderosa pine and mixed conifer forest structure in the Southern Sierra Nevada. *Ecosphere*,
787 6, 1–63.

788 99.

789 Sugihara, N.G. & Barbour, M.G. (2006). Fire and California vegetation. In: *Fire in california's ecosystems*
790 (eds. Sugihara, N.G., Van Wagtendonk, J.W., Shaffer, K.E., Fites-Kaufman, J. & Thode, A.E.). University
791 of California Press, Berkeley; Los Angeles, CA, USA, pp. 1–9.

792 100.

793 Tilman, D. (1994). Competition and biodiversity in spatially structured habitats. *Ecology*, 75, 2–16.

794 101.

795 Trumbore, S., Brando, P. & Hartmann, H. (2015). Forest health and global change. *Science*, 349.

796 102.

797 Tuanmu, M.-N. & Jetz, W. (2015). A global, remote sensing-based characterization of terrestrial habitat
798 heterogeneity for biodiversity and ecosystem modelling. *Global Ecology and Biogeography*, n/a–n/a.

799 103.

800 USGS. (2017a). Product Guide: Landat 8 Surface Reflectance Code (LaSRC) Product. *USGS Professional*
801 *Paper*, 4.2.

802 104.

803 USGS. (2017b). Product Guide: Landsat 4-7 Surface Reflectance (LEDAPS) Product. *USGS Professional*
804 *Paper*, 8, 38.

805 105.

806 Vehtari, A., Gelman, A. & Gabry, J. (2016). Practical Bayesian model evaluation using leave-one-out
807 cross-validation and WAIC. *Statistics and Computing*, 1–20.

808 106.

809 Veraverbeke, S. & Hook, S.J. (2013). Evaluating spectral indices and spectral mixture analysis for assessing
810 fire severity, combustion completeness and carbon emissions. *International Journal of Wildland Fire*, 22,
811 707–720.

812 107.

813 Vermote, E., Justice, C., Claverie, M. & Franch, B. (2016). Preliminary analysis of the performance of the
814 Landsat 8/OLI land surface reflectance product. *Remote Sensing of Environment*, 185, 46–56.

815 108.

816 Virah-Sawmy, M., Willis, K.J. & Gillson, L. (2009). Threshold response of Madagascar's littoral forest to
817 sea-level rise. *Global Ecology and Biogeography*, 18, 98–110.

818 109.

819 Walker, B., Holling, C.S., Carpenter, S.R. & Kinzig, A. (2004). Resilience, adaptability, and transformability
820 in social-ecological systems. *Ecology and Society*, 9, 5.

821 110.

822 Walker, R.B., Coop, J.D., Parks, S.A. & Trader, L. (2018). Fire regimes approaching historic norms reduce
823 wildfire-facilitated conversion from forest to non-forest. *Ecosphere*, 9.

824 111.

825 Westerling, A.L., Hidalgo, H.G., Cayan, D.R. & Swetnam, T.W. (2006). Warming and earlier spring increase
826 western U.S. forest wildfire activity. *Science*, 313, 940–943.

827 112.

828 Wood, E.M., Pidgeon, A.M., Radeloff, V.C. & Keuler, N.S. (2012). Image texture as a remotely sensed
829 measure of vegetation structure. *Remote Sensing of Environment*, 121, 516–526.

830 113.

831 Young, D.J.N., Stevens, J.T., Earles, J.M., Moore, J., Ellis, A. & Jirka, A.L. *et al.* (2017). Long-term climate
832 and competition explain forest mortality patterns under extreme drought. *Ecology Letters*, 20, 78–86.

833 114.

834 Zhu, Z., Key, C., Ohlen, D. & Benson, N. (2006). Evaluate Sensitivities of Burn-Severity Mapping Algorithms
835 for Different Ecosystems and Fire Histories in the United States. *Final Report to the Joint Fire Science*
836 *Program, Project JFSP 01-1-4-12*, 1–35.